CONF-9507167--2

UCRL-JC-120839
PREPRINT

Classical Rayleigh Taylor Experiments on Nova

K. S. Budil, B. A. Remington, T. A. Peyser, K. O. Mikaelian, P. L. Miller,
N. C. Woosley, M. M. Marinak, H. Louis, T. Demiris, R. Wallace, W. M. Wood-Vasey

This paper was prepared for submittal to the
5th International Workshop on Compressible Turbulent Mixing
Stony Brook, NY
July 18-21, 1995

July 1995

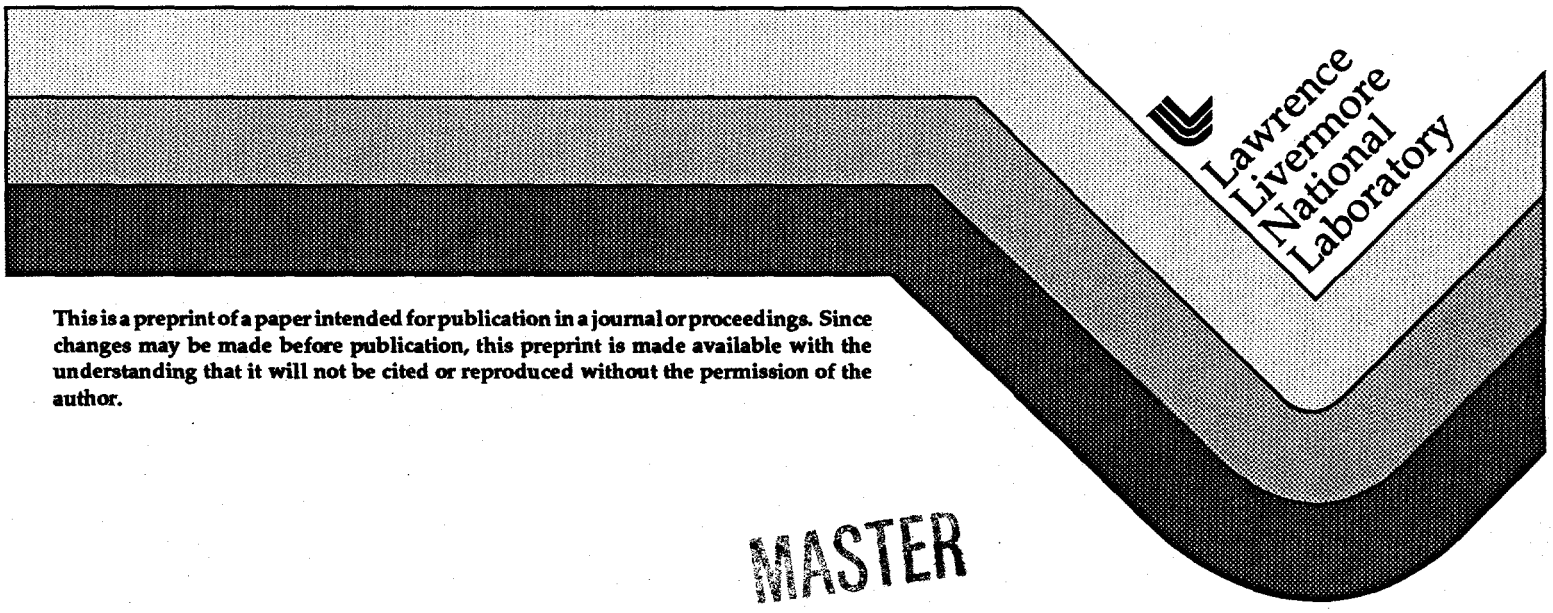

This is a preprint of a paper intended for publication in a journal or proceedings. Since changes may be made before publication, this preprint is made available with the understanding that it will not be cited or reproduced without the permission of the author.

MASTER

DISTRIBUTION OF THIS DOCUMENT IS UNLIMITED

DISCLAIMER

This document was prepared as an account of work sponsored by an agency of the United States Government. Neither the United States Government nor the University of California nor any of their employees, makes any warranty, express or implied, or assumes any legal liability or responsibility for the accuracy, completeness, or usefulness of any information, apparatus, product, or process disclosed, or represents that its use would not infringe privately owned rights. Reference herein to any specific commercial products, process, or service by trade name, trademark, manufacturer, or otherwise, does not necessarily constitute or imply its endorsement, recommendation, or favoring by the United States Government or the University of California. The views and opinions of authors expressed herein do not necessarily state or reflect those of the United States Government or the University of California, and shall not be used for advertising or product endorsement purposes.

DISCLAIMER

Portions of this document may be illegible in electronic image products. Images are produced from the best available original document.

Classical Rayleigh Taylor Experiments on Nova*

K.S. Budil, B.A. Remington, T.A. Peyser, K.O. Mikaelian, P.L. Miller, N.C. Woosley, M.M. Marinak, H. Louis, T. Demiris, R. Wallace

Lawrence Livermore National Laboratory
Livermore, CA 94550

and

W. M. Wood-Vasey

Harvey Mudd College
Claremont, CA 91711

In preparation for submittal to
5th International Workshop on Compressible Turbulent Mixing, Stony Brook, NY, July 18-21,1995

Abstract

The evolution of the Rayleigh-Taylor (RT) instability in a compressible medium was investigated both at an accelerating embedded interface and at the ablation front in a new series of experiments on Nova. The x-ray drive generated in a hohlraum ablatively accelerated a planar target consisting of a doped plastic pusher which was in some cases backed by a higher density titanium payload. Both target types were diagnosed by face-on and side-on radiography. Experiments have been done with a variety of wavelengths and initial amplitudes. In the case where the perturbed RT-unstable embedded interface is isolated from the ablation front, short wavelength perturbations are observed to grow strongly. When the perturbation is at the ablation front, the short wavelengths are observed to be severely stabilized. *This work was performed under the auspices of the U. S. Department of Energy by the Lawrence Livermore National Laboratory under Contract No. W-7405-ENG-48.

MASTER

We are surrounded with examples of the Rayleigh-Taylor[Ch68] (RT) instability every day. One need go no further than the kitchen sink to assemble a closed jar partially filled with colored water topped off with mineral oil (lower density). When the jar is quickly turned over, one has a heavy fluid "sitting on top of" a lighter fluid. The RT- or fluid interchange instability is the mechanism by which the interface evolves, causing "spikes" of the higher density fluid to penetrate the lower density fluid and "bubbles" of the lower density fluid to rise through the heavier layer. Occurrences of this interface instability are ubiquitous in nature. By turning one's eye to the sky, this situation can be observed in the evolution of the contrails of a jetliner, with spikes of the heavier water vapor falling through the less dense atmosphere. Astrophysics is replete with examples of the RT instability, and its shock analog, the Richtmyer-Meshkov[Ri60] (RM) instability. A good example is the occurrence of strong RT-driven mix in the evolution of Supernova 1987A.[Mu91,He94] On a more "down-to-earth" front, the RT instability is considered the *bête noire* of inertial confinement fusion[Ha89] (ICF). As an ICF capsule is ablatively imploded, first the ablation front is RT unstable during the acceleration, followed by the pusher-fuel interface during deceleration and stagnation. Strong RT growth can severely degrade capsule performance. In ICF, a clear distinction has been drawn between classical versus ablative RT evolution. Stabilization effects due to ablation and also density gradients have been posited and studied theoretically and numerically. With little exaggeration one could say that the fate of ICF depends critically on the notion of ablative stabilization. We present here the first direct experimental verification of ablative stabilization by comparing the RT evolution of a classical interface with that at the ablation front under similar conditions. Strong stabilization of the short wavelength perturbations is observed at the ablation front, whereas the shortest wavelength perturbations grow the most at the classical interface.

The experimental configuration is shown in Fig. 1 and is described in more detail elsewhere.[Re95] A 750 μm diameter planar package is mounted across a diagnostic hole on a 3 mm long, 1.6 mm diameter gold cylindrical hohlraum. Eight of the 10 Nova laser beams are used at λ=0.351 μm to generate a 3.3 ns low-adiabat, shaped drive, as shown in Fig. 2a. Two 3 ns square beams at λ=0.528 μm are delayed by 2 ns relative to the drive and focused onto either an iron (for the classical interface experiments) or

molybdenum (for the ablation front experiments) backlighter disk to generate 6.7 keV He-α x-rays from Fe or 2.6 keV L-band x-rays from Mo to back-illuminate the accelerating planar foil. Random phase plates with 5 mm diameter hexagonal elements are inserted as the last optic in the two backlighter lasers to generate a smooth 700 μm diameter x-ray spot. On each laser shot, two-dimensional gated x-ray images were obtained with a new flexible gated x-ray pinhole camera.[Bu95] Four gated pinhole images are obtained for each strip on the MCP, and the interstrip delay was set to 700 ps. For the classical interface experiments, half of the pinholes on each strip were filtered with 12.5 μm of Fe to eliminate any possible higher energy backlighter x-rays such as from He-β and He-γ transitions in Fe. No significant difference was observed in images analyzed with or without the Fe filter. For the ablation front experiments, a 1 μm Ag filter was used over half the pinholes.

Two types of target were investigated. The embedded interface targets consisted of a 35 μm thick CH(Br) ablator ($C_{50}H_{47}Br_3$, ρ=1.26 g/cm^3) backed by a 15 μm thick Ti payload. Sinusoidal ripples were placed at the CH(Br)-Ti interface corresponding to (on separate shots) wavelengths of λ=20, 50, and 100 μm and amplitudes of η_0= 0.5, 1.0, and 2.0 μm. The targets were made by machining the sinusoidal groves into copper disks, which were then sputter coated with Ti, whose back side was polished flat. The Cu mandrel was acid-etched away, and the 35 μm CH(Br) was hot-pressed onto the rippled Ti surface. The ablation front experiments used thicker (50-60 μm) CH(Br) foils with no Ti payload, and had the ripples molded onto the ablation front side.

The drive used is illustrated in Fig. 2a,b and is discussed extensively elsewhere.[Re95] In brief, the hohlraum radiation temperature was characterized (1) by doing shock trajectory measurements in calibrated wedged "witness-plate" targets of Al mounted on the hohlraum wall, and (2) by making foil trajectory measurements in side-on geometry. Such foil trajectory experiments were conducted for each type of target (embedded interface and ablation front), and the result for the CH(Br)-Ti composite foil is shown in Fig. 2b, along with the result from a 1D radiation-hydrodynamics code HYADES[La92]. The trajectory results for the ablation front foils can be found in refs. Re92, Re95.

In Fig. 3 we show sample raw images that illustrate the essence of this investigation. Across the top row are images taken early in time, at 2.5 ns, of (a) the λ=20 μm perturbation and (b) the λ=50 μm perturbation at the

embedded interface, and (c) a side-by-side λ=20 μm and λ=50 μm perturbation at the same ablation front of a single foil. Figures 3d-f show results from the same accelerated foils only late in time (4.5 ns). The perturbation initial amplitudes in all cases here were η_o=1 μm. Strong growth of the short wavelength perturbation at the embedded interface is clearly observed, evidenced by the distinct contrast in the image. This is in marked contrast to the ablation front experiment, where growth is only observed for the λ=50 μm perturbation, with no contrast evident from the λ=20 μm perturbation, even though both perturbations experience identical drive conditions and had the same initial amplitude. Note, the drive for both the embedded interface experiments and the ablation front experiments was identical. Qualitatively, we can conclude from the raw data alone that there is a striking difference between growth at a classical interface versus at the ablation front.

In Fig. 4a we show the growth factor for the fundamental mode of ℓn(exposure) $\propto -\delta\int\rho\cdot dz$ for the embedded interface experiments. The λ=20 μm perturbation clearly exhibits the highest growth factor, ~12, compared to a growth factor of approximately 2.5 for λ=50 μm at the same time, and $\leq$ 1.5 for λ=100 μm for the embedded interface perturbation. The corresponding values for the ablation-front experiment are GF≈20 for the λ=50 μm perturbation and GF $\leq$ 2 for the λ=20 μm ripple. Note that at the classical interface, the growth at λ=20μm is a factor of ~5 <u>higher</u> than that at λ=50μm at the same time, whereas for the ablation front experiment, the growth at λ=20μm is more than a factor of 5 <u>lower</u> than that at λ=50μm.

We compare the classical RT evolution of the embedded interface with the physically intuitive model of Alon *et al.*,[Al95] using the 1D code HYADES[La92] to generate the gross foil hydrodynamics. The 1D simulations reproduce the foil trajectory very well, as shown in Fig. 2b. For simplicity, we assume that the exponential growth due to the Rayleigh-Taylor instability dominates the growth due to the Richtmyer-Meshkov instability which is linear in time. Hence, we concentrate on modeling the perturbation growth only after the foil starts to accelerate as a unit at $t=t_1$=2.9 ns. We assume that the RT growth remains in the linear regime until its spatial amplitude exceeds 10% of its wavelength. The perturbation spatial amplitude at the start of our calculation, $t=t_1$, is estimated by

$$\eta(t_1) = GF_{exp}(t_1)*\eta_o(\mu m)*\rho_o/\rho(t_1), \qquad (1)$$

where $GF_{exp}(t_1)$ is the experimental growth factor at the moment the foil starts to accelerate, $\eta_o(\mu m)$ is the initial perturbation amplitude at t=0, ρ_o is the initial density of the Ti, and $\rho(t_1)$ is the density of the Ti at the interface at $t=t_1$. Note, the ratio $\rho(t_1)/\rho_o$ represents the Ti compression at $t=t_1$. We calculate the GF during the linear RT regime by

$$GF(t) = e^{\int \gamma \cdot dt} , \qquad (2)$$

where $\int \gamma \cdot dt$ represents the classical RT e-foldings from time t_1 to t. We assume a growth rate, γ, given by

$$\gamma^2 = [Akg/(1+kL)]^{1/2} * f_c , \qquad (3)$$

where $A = (\rho_1-\rho_2)/(\rho_1+\rho_2)$ represents the Atwood number at the CH(Br)-Ti interface [1=Ti, 2=CH(Br)], $k=2\pi/\lambda$ is the perturbation wavenumber, g is the acceleration of the interface, and $L=\rho/\nabla\rho$ is the density gradient scale length. Note that this form has the correct limiting behavior as $L \rightarrow 0$. The reduction factor, f_c, is due to the finite thickness of the Ti foil. This correction is given by[LL87, Re92]

$$f_c = (1-r)/[1+r*\coth(kh)] , \qquad (4)$$

where $r=\rho_2/\rho_1$ is the ratio of fluid densities ($\rho_2 < \rho_1$), and h is the layer thickness of the Ti foil. All of the parameters for Eq. 3 are time dependent, and taken from the 1D simulations. Similar to the situation at $t=t_1$, we estimate the perturbation spatial amplitude as a function of time by

$$\eta(t) = GF(t)*\eta(t_1)*\rho(t_1)/\rho(t) . \qquad (5)$$

When $\eta(t) \geq 0.1\lambda$, we then switch smoothly to the asymptotic RT limit of terminal bubble velocity, u_B, given in ref. ( ) by

$$u_B = [2g\lambda A/(1+A)]^{1/2} . \qquad (6)$$

To ensure a smooth transition from the linear regime to this asymptotic limit in the nonlinear regime, we require that the bubble velocity vary smoothly across the transition time. We accomplish this by writing

$$d\eta/dt = \gamma\eta\,, \text{ for } t \le t_1 \qquad (7)$$

$$d\eta/dt = \gamma(t_1)\eta(t_1)*f_s(t), \text{ for } t > t_1$$

where the scaling ratio $f_s(t)$ is derived from Eq. 6 as

$$f_s(t) = \{ [g(t)A(t)/(1+A(t))]/[g(t_1)A(t_1)/(1+A(t_1))] \}^{1/2}. \qquad (8)$$

The results of these calculations are shown by the smooth curves in Fig. 4a. We see that the RT growth at this compressible but classical interface is reproduced reasonably well by this simple model.

For the ablation-front growth, we adopt another intuitive model, namely, a modified Takabe approach.[Ta83] For the linear RT regime, we approximate the growth rate as[We94]

$$\gamma = [kg/(1+kL)]^{1/2} - \beta k v_a\,, \qquad (9)$$

where k, g, and L are as defined above, β is an adjustable parameter here set to β=2, and $v_a=(dm/dt)/\rho_{max}$ is the ablation velocity. The time-dependent values of all the parameters in Eq. 9 are taken from the 1D hydrodynamics simulation. The correction for the finite layer thickness (Eq. 4) is small and is neglected. The observations show that the RT evolution did not significantly enter the nonlinear regime, so the analysis is restricted to linear regime only. We compare the calculated GF's with the observed growth after shock breakout, as shown by the smooth curves in Fig. 4b. Qualitatively, this simple model does a reasonable job of reproducing the features observed in the data.

To make the comparison of ablation-front RT growth versus growth at the embedded interface, we use ratios. In Fig. 5 we show the ratio of GF at t=4 ns for each wavelength studied to the corresponding GF at λ=100 μm, both for the classical interface and for the ablation front. For the ablation-front case, we have added values from a previous investigation using the same drive but a different diagnostic.[Re95] The smooth curves represent the

corresponding values for the calculations described above. The difference in the behavior of this ratio, GF(λ)/GF(λ=100μm), between the classical interface and the ablation front is indeed striking. For the classical interface, the λ=20μm perturbation grows a factor of 5 times larger than the λ=50μm perturbation, and a factor of 10 times larger than the λ=100μm perturbation, in agreement with the classical analysis. Whereas, for the ablation-front case, the growth peaks at λ=50μm, and the growth at λ=20μm is only a fraction of that observed at λ=50μm. The reason for this striking difference is the large ablation velocity in indirect-drive and the density gradient scalelength at the ablation front. For perturbation wavelengths shorter than about 30μm, the RT growth is strongly stabilized at the ablation front. To our knowledge, this is the first unambiguous experimental demonstration of the stabilizing effect on RT growth at an ablation front. This striking demonstration was realized by comparing growth at the ablation front directly to growth at an embedded interface, remote from the effects of ablation.

Figure Captions:

Figure 1: Experimental configuration

Figure 2: (a) Typical total laser power, and corresponding radiation drive temperature. (b) The corresponding foil trajectory (experimental and 1D simulation) for the drive shown in (a), and the deduced interface acceleration profile, based on 1D hydrodynamics simulations for the embedded interface.

Figure 3: Images of the "raw" film density data. (a) Image of the λ=20μm perturbation, embedded interface foil at 2.5 ns. (b) Same, only for the λ=50μm perturbation. (c) Same, only for the ablation-front foil with λ=20μm side-by-side with λ=50μm on the same foil. (d-f) Show the same perturbations (λ=20μm, λ=50μm, and λ=20+50μm side-by-side) at t=4.6 ns.

Figure 4: (a) Growth factor of the fundamental mode of contrast vs time for the λ=20, 50, and 100 μm perturbation at the embedded interface. (b) Same, only for growth at the ablation front. The solid curves in (a) correspond to

the result of a classical RT growth calculation, and in (b) to a calculation with the Takabe relation.

Figure 5. Ratios of GF at 4 ns at the various wavelengths vs GF at λ=100μm for the embedded interface and ablation front. The smooth curves correspond to the calculations shown in Fig. 4.

References:

Ch68: S. Chandrasekhar, *Hydrodynamic and Hydromagnetic Stability* (Oxford University Press, London, 1968), Chap. 10.

Mu91: E. Muller, B. Fryxell, and D. Arnett, Astorn. Astrophys. **251**, 505 (1991);

R.D. Richtmyer, Commun. Pure Appl. Math. **13**, 297 (1960); E.E. Meshkov, Izv. Akad. Nauk. SSSR, Mekh. Zhidk. Gaz. **5**, 151 (1969) (NASA TTF-13-074, 1970).

He94: M. Herant and S.E. Woosley, Ap. J. **425**, 814 (1994).

Ha89: S.W. Haan, Phys. Rev. A **39**, 5812 (1989).

Re95: B.A. Remington *et al.*, Phys. Plasmas **2**, 255 (1995).

Bu95: K.S. Budil *et al.*, submitted, Rev. Sci. Instrum. (1995).

La92: Jon Larsen, proceedings, Sarasota conference on high energy density physics (1992).

Re92: B.A. Remington *et al.*, Phys. Fluids B **4**, 967 (1992).

Al95: U. Alon, J. Hecht, D. Ofer, and D. Shvarts, Phys. Rev. Lett. **74**, 534 (1995).

LL87: L.D. Landau and E.M. Liftshitz, *Fluid Mechanics*, 2nd ed. (Pergamon, new York, 1987), Sec. 12, p. 36, problem 3.

Ta83: H. Takabe *et al.*, Phys. Fluids **26**, 2299 (1983); *ibid*, **28**, 3676 (1985).

We94: S.V. Weber *et al.*, Phys. Plasmas **1**, 3652 (1994).

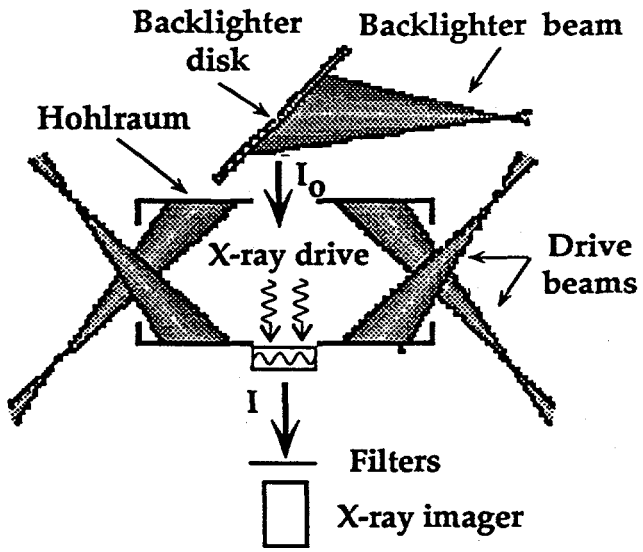
Backlighter disk
Backlighter beam
Hohlraum
I_0
X-ray drive
Drive beams
I
Filters
X-ray imager

Fig. 1

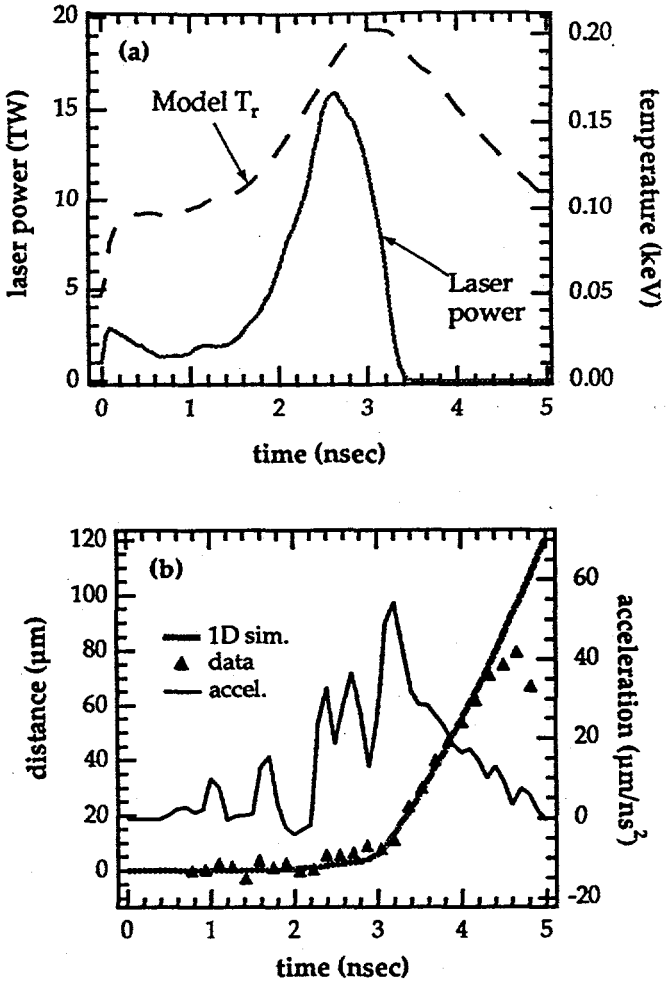
(a)
Model T_r
Laser power
laser power (TW)
temperature (keV)
time (nsec)
(b)
1D sim.
data
accel.
distance (μm)
acceleration (μm/ns²)
time (nsec)

Fig. 2

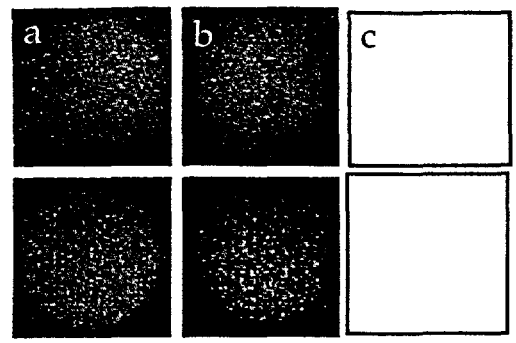

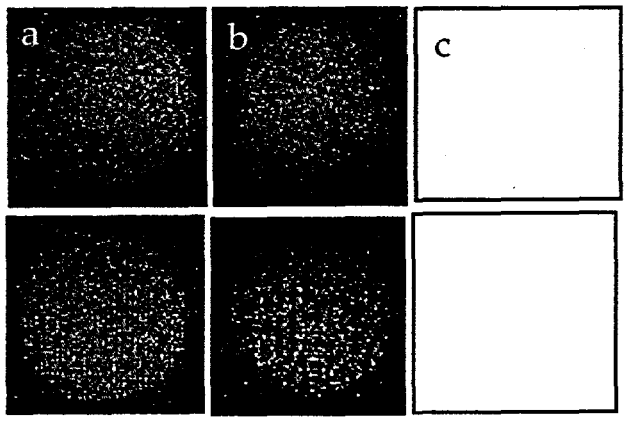

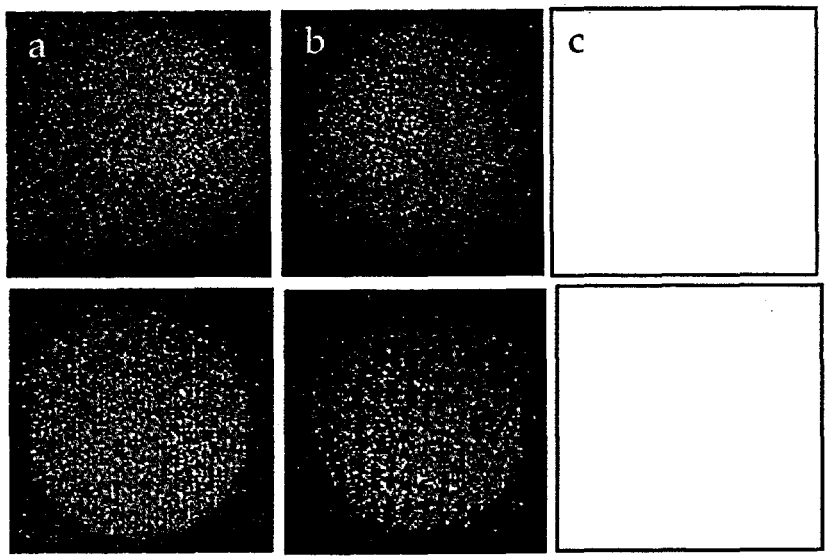

Fig. 3

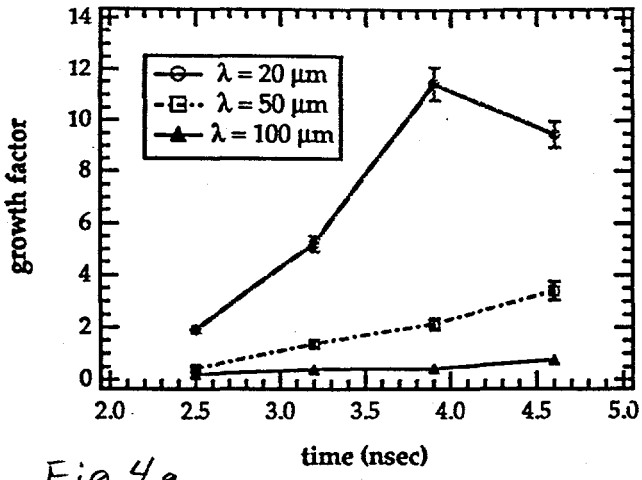

Fig 4a

Same, only for abl. front

Fig. 4b

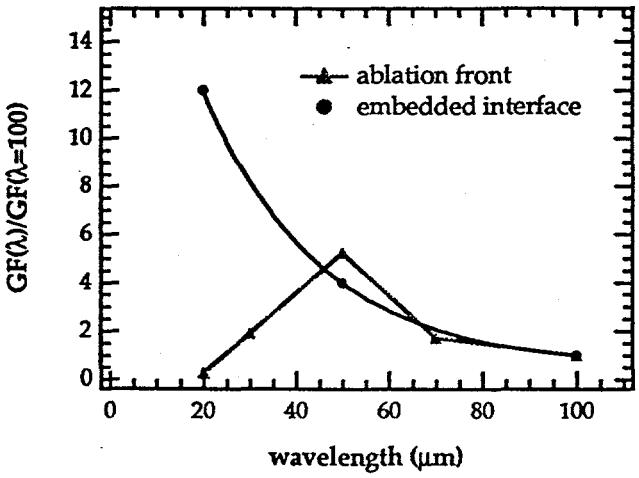

Fig. 5